THE TESLA DETECTOR

S. SCHREIBER

Deutsches Elektronen-Synchrotron, 22603 Hamburg, Germany

Abstract. The joint ECFA/DESY Study "Physics and Detectors for a Linear Collider" has worked out a proposal for a detector for a next generation TeV e^+e^- linear collider. In this report, the principle design and layout of the proposed detector with emphasis on the TESLA version is reviewed. Examples of reference reactions studied to demonstrate the detector performance are given.

Presented at the 2nd Workshop on Electron-Electron Interactions at TeV Energies, Santa Cruz, CA (U.S.A.), September 22-24, 1997.

THE TESLA DETECTOR

S. SCHREIBER
Deutsches Elektronen-Synchrotron, 22603 Hamburg, Germany

The joint ECFA/DESY Study "Physics and Detectors for a Linear Collider" has worked out a proposal for a detector for a next generation TeV e^+e^- linear collider. In this report, the principle design and layout of the proposed detector with emphasis on the TESLA version is reviewed. Examples of reference reactions studied to demonstrate the detector performance are given.

1. Introduction

The next generation linear e^+e^-colliders will be essential instruments to explore particle physics in the energy range up to the TeV scale and to search for fundamental constituents of matter and their interactions. The joint ECFA/DESY Study "Physics and Detectors for a Linear Collider" has worked out a proposal for a detector which matches the requirements of the physics analyses to thoroughly realize the full physics potential of the linear collider. The result of this study is summarized in a conceptual design report.[1]

TESLA is an international collaboration for a TeV linear collider which uses a superconducting acceleration technology. Emphasis will be the exploitation of positron electron collisions well beyond the reach of LEP. In an initial phase, it is planned to reach a center of mass energy of 350 to 500 GeV with a luminosity above $5{\cdot}10^{33}\,\mathrm{cm}^{-2}\mathrm{s}^{-1}$. Provisions are being made to build a second interaction region, which could be used for e^-e^-, $e^-\gamma$, and $\gamma\gamma$-collisions.

In this report, the detector concept proposed for TESLA and an overview of the major detector components is given.

2. Basic Detector Requirements and Layout Concept

To fully explore the physics potential up to the TeV scale the detector will be designed as a multi-purpose detector. The key components of the detector have to meet excellent performance in most of the physics analysis aspects. A very good vertex resolution is required for heavy flavor tagging. Important for jet-jet reconstructions is a high 3D granularity and redundancy of the main tracker and the calorimeters, as well as a good energy flow measurement, supported by a very good momentum resolution together with a good particle identification in the trackers. The measurement of missing energy, essential for new particle searches, demands a good hermeticity and a good coverage of the forward region. In addition the detector should have a very good lepton identification and e-π separation. The trigger must

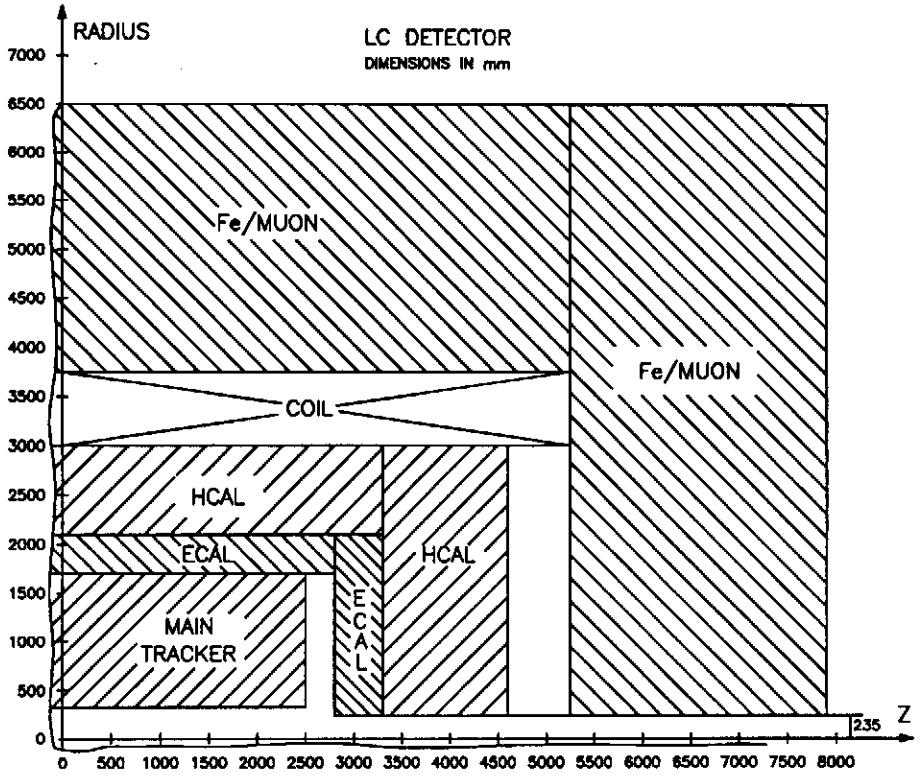

Fig. 1. Schematical layout of one quadrant of the detector.

be flexible in order to cope with the various backgrounds mostly induced by the collider operation.

The basic detector layout follows the well-proven concept of tracking particles in a magnetic field first and than measuring their energy in a calorimeter. A schematic layout of the major detector components is shown in Fig. 1. Table 1 shows the principle detector subsystems together with the proposed detector type, their resolution and performance goals obtained from physics analyses.

The detector magnet will be a superconducting solenoid with a field of 3 T. The coil will be large enough to have the electromagnetic and a large part of the hadronic calorimeter inside the coil. The magnet serves not only to measure particle momenta, but also confines background particles from beam-beam interactions inside a narrow cone towards the forward region. This makes it possible to shield the detector by a conical shaped masking system.

With a nominal luminosity of $5 \cdot 10^{33}\,\mathrm{cm}^{-2}\mathrm{s}^{-1}$, an integrated luminosity of $50\,\mathrm{fb}^{-1}$ is collected in 100 days. The event rates are rather modest: e.g. 3200 Bhabha, 140 $\mathrm{W^+W^-}$, 63 $\mathrm{q\bar{q}}$, and 15 $\mathrm{t\bar{t}}$ events per hour are expected. Due to the good shielding of the mask, background events are much reduced: only 31 $\mathrm{e^+e^-}$ and $3 \cdot 10^{-3}$ $\gamma\gamma$ and minijet events are expected per hour (all numbers for $\sqrt{s} = 500\,\mathrm{GeV}$).

Table 1. Principle detector components, their radiation or interaction lengths, the proposed detector techniques, and their resolution or performance goals.

Subdetector	Rad. Length	Technique	Performance goal
Barrel			
Beam pipe	0.3 % X_0	Beryllium	$\delta(\mathrm{IP}_{r\phi}) \leq 10\,\mu\mathrm{m} \oplus 30\,\mu\mathrm{m}/p\sin^{3/2}\theta$
Vertex detector	1.6 % or 2.4 % X_0	CCD or APS	$\delta(\mathrm{IP}_z) \leq 20\,\mu\mathrm{m} \oplus 30\,\mu\mathrm{m}/p\sin^{5/2}\theta$
Intermediate tracker	0.23 % X_0	Honeycomb chamber	(p in GeV/c)
Intermediate layer	1 % X_0	Double-sided silicon strips	
Main tracker	3 % X_0	Time projection chamber	$\delta p_t/p_t^2 \leq 2.8{\cdot}10^{-4}\,(\mathrm{GeV}/c)^{-1}$
Combined Trackers	6.1 % X_0 (CCD)		$\delta p_t/p_t^2 \leq 1{\cdot}10^{-4}\,(\mathrm{GeV}/c)^{-1}$
Presampler	1.6 X_0	Scintillating fibers	
Elm. Calorimeter	27 X_0, 1.1 λ	Pb-scintillator shashlik	
Combined ECAL	28.6 X_0, 1.1 λ		$\delta E/E \leq 0.10\frac{1}{\sqrt{E}} \oplus 0.01$ (E in GeV)
			Granularity $0.9^\circ \times 0.9^\circ$
Had. Calorimeter	4.7 λ	Cu-scintillator shashlik	
Coil	0.9 λ	Al, Scint. pads	3 T
Muon detector, Tailcatcher	11 λ	Resistive plate chambers	$\delta p/p < 20\,\%$
Combined HCAL	16.6 λ		$\delta E/E \leq 0.50\frac{1}{\sqrt{E}} \oplus 0.04$ (E in GeV)
			Granularity $2^\circ \times 2^\circ$
Forward/Endcap			
Luminosity calorimeter		Scintillating fibers in Pb	$\delta\int\mathcal{L}dt/\int\mathcal{L}dt < 0.1\,\%$
Instrumented mask		Quartz fibers in W	
Forward tracker		Silicon strip and/or pixels	$\delta p/p < 20\,\%$, $\delta_\theta < 200\,\mu$rad
			for 100 to 250 GeV particles
Forward muon tracker		Toroids with honeycomb/straw tubes	$\delta p/p < 20\,\%$
Elm. Calorimeter	27 X_0, 1 λ	Pb-scintillator shashlik	see barrel
Had. Calorimeter	10 λ	Cu-scintillator shashlik	see barrel
Energy Flow			$\delta E/E \simeq 0.3\frac{1}{\sqrt{E}}$ (E in GeV)
Hermetic Coverage			$\lvert\cos\theta\rvert < 0.99$

TESLA-Report 1998-03

3. The Tracking System

The tracking system consist of a series of inner detectors and the main tracker. The inner detectors measure the vertices and perform the matching to the main tracker, which – combined with the inner detectors – measures momentum, resolves jets and identifies particles. The design of the inner detectors are largely influenced by the design of the TESLA interaction region and the background conditions.

The main source of background is induced by beam-beam interaction: hard synchrotron radiation (beamstrahlung) is emitted and degrades the energy distribution, reduces and spreads the center-of-mass energy. A strong background of photons and low energy e^+e^- particles are produced. Also remnants of hard bremsstrahlung events of the incoming beam and low energy hadronic events contribute to the background. The beamstrahlung itself is emitted in a narrow cone and exits the detector through the beam pipe. To shield the detector against these background sources, a special masking system is proposed. For details on the TESLA interaction region layout, the expected background, and a description of the masking system, see also Ref. 2.

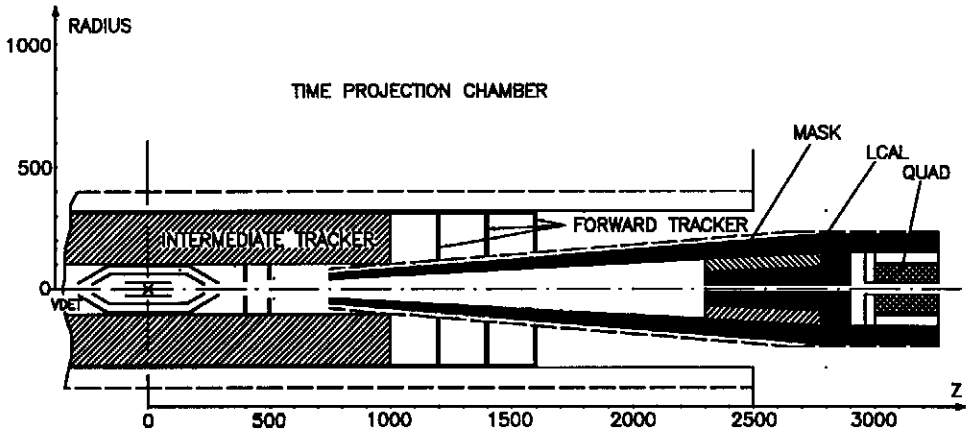

Fig. 2. Schematic layout of the inner region of the detector. The scale shown is in mm.

The mask covers the forward region, because most particles are emitted within an angle of less than 55 mrad, mostly due to the 3 T solenoid field of the detector magnet. The inner part of the mask has a radius of 18 mm determined by the collimation system. It shields the innermost layers of the vertex detector against background backscattered from the final focus quadrupoles and other sources, e.g. neutrons from electromagnetic showers induced by the beamstrahlung in the collimators about 100 m from the interaction point. In order to be in the shadow of the mask, the beam pipe and the vertex detector radii have to be larger than the mask clearance (see Fig. 2). A beam pipe radius of 20 mm and a radius of 25 mm for the first vertex detector layer was chosen. Figure 3 shows the number of charged particles hitting the vertex detector as a function of its radius. Note, that in average

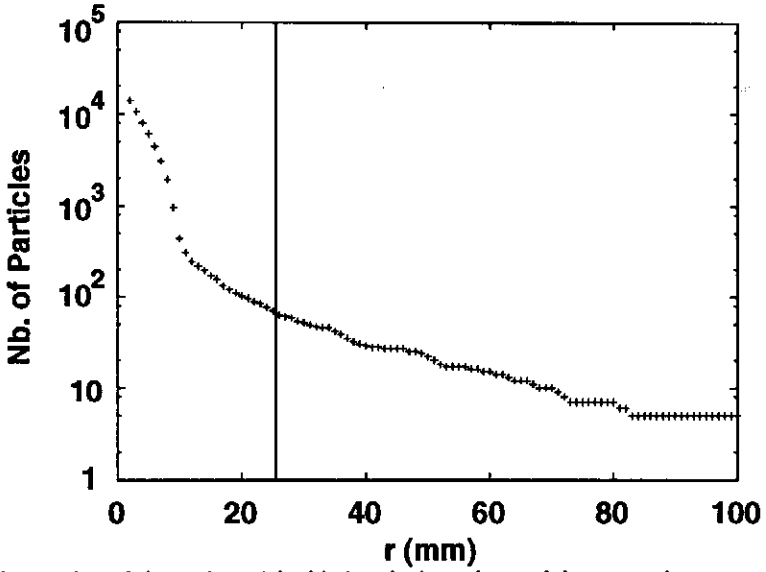

Fig. 3. The number of charged particles hitting the inner layer of the vertex detector as a function of its radius for an angular coverage of $|\cos\theta| < 0.98$ and a solenoid field of 3 T (TESLA 500 GeV c.m. parameters). Indicated is the chosen position of the inner vertex detector layer.

one particle produces 3 hits in the first layer. With a solenoid field of 3 T, 230 hits per bunch crossing are produced for a radius of 25 mm. This corresponds to 10^{-2} hits per mm^2. Reducing the field to 2 T would double the number of hits.[3]

The inner detectors consist of three types: a vertex detector of three layers of charge coupled devices (CCD) or active pixel sensors (APS), an intermediate tracker of honeycomb chamber tubes, and an outer part of double sided silicon strips as an intermediate layer. The intermediate layer improves the track matching to the main tracker. Figure 2 shows the proposed inner detector layout. The intermediate trackers are extended to the forward region with disks of pixel and silicon-strip detectors. The minimal azimuthal angle is $\theta = 5°$ given by the mask design. It is planned to instrument the inner part of the mask and the far forward region, which would significantly improve the hermeticity. A small angle calorimeter would serve also for tagging $\gamma\gamma$ events. It should be pointed out, that the forward coverage is already close to the requirements for the e^-e^-case.

The performance of the vertex detector can be illustrated by the b- and c-tagging purity (Fig. 4). Significant gain can be made by reducing the pixel size and the material thickness, and by choosing a smaller beam pipe radius. The latter requires an optimization of the TESLA collimation system, which is possible if necessary.

A time projection chamber (TPC) as the main tracker was chosen. It has a very small radiation length (3 % for the inner field cage plus gas) and a much better z resolution as jet chamber designs. It has a very high granularity (10^8 3D-pixels) and tracking redundancy, which is essential for good multijet physics. The occupancy from background is estimated to be at most 0.4 %. It also has good

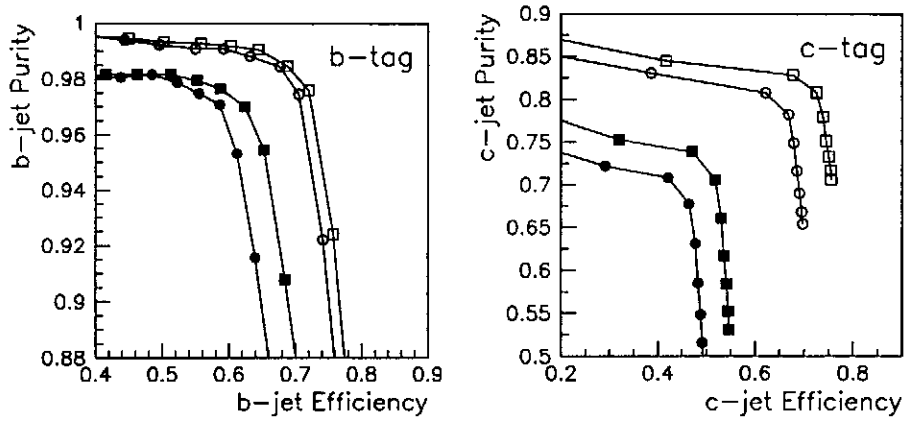

Fig. 4. Purity for bottom (a) and charm (b) identification with the vertex detector in 50 GeV jets as a function of its efficiency. Open squares and circles refer to the CCD option, with a beam pipe radius of $r = 10$ and 22 mm respectively. The filled squares and circles refer to the APS option for the same beam pipe radii.

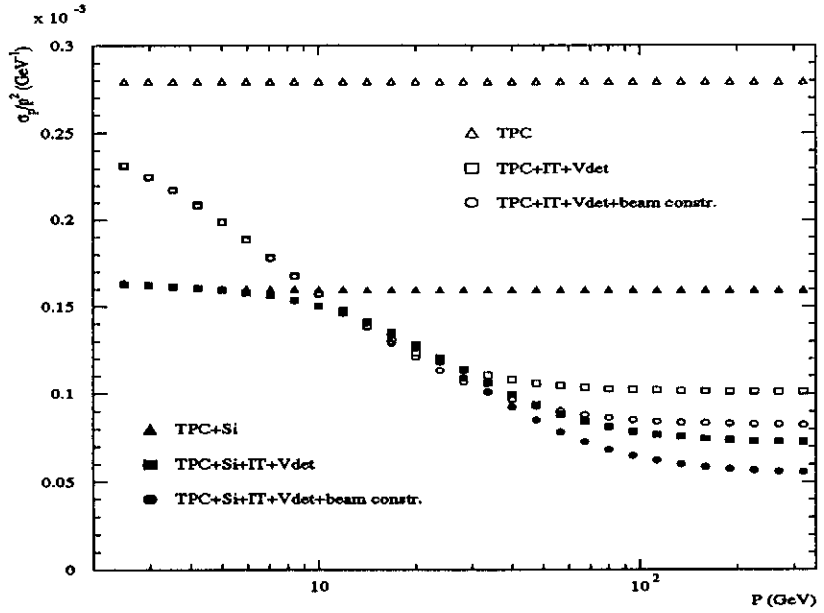

Fig. 5. Momentum resolution of $\delta p/p^2$ for 90° tracks for various detector combinations. An APS vertex detector is assumed. (Vdet = vertex detector, IT = intermediate tracker, Si = intermediate silicon layer)

$r\phi$-resolution and allows a good dE/dx measurement. A momentum resolution of $\delta p/p^2 = 2.8{\cdot}10^{-4}(\mathrm{GeV}/c)^{-1}$ is expected. The improvement by a factor of 4 compared to the ALEPH TPC[4] is mainly due to the higher magnetic field by a factor of 2 and an increase of the number of points per track by a factor of 6. The resolution will be significantly improved using the inner trackers. Figure 5 shows the

momentum resolution for various detector combinations. Combining all trackers, a resolution below $10^{-4}(\mathrm{GeV}/c)^{-1}$ is achieved.

4. Calorimetry

The tracking system is followed by a set of calorimeters to measure the energy of charged and neutral particles. It is divided in the electromagnetic part followed by a hadronic calorimeter. Both are inside the superconducting coil (see Fig. 1). The coil represents about one nuclear interaction length of dead material and would therefore degrade the resolution. The iron return yoke is instrumented to detect muons and to complete the hadronic energy flow measurement.

For both calorimeter parts, a shashlik-type tower structure was chosen, because its homogeneous, compact and hermetic. It consists of sandwiched layers of absorber and scintillator material with wavelength shifters and fiber-readout. For the electromagnetic part, lead is chosen as the absorber material, the hadronic part uses copper absorbers. The electromagnetic calorimeter has 30 layers of lead/scintillator sheets, both with a thickness of 5 mm corresponding to 27 radiation lengths X_0 in total. The interaction length λ is 30 cm. The hadronic part has 33 layers of copper/scintillator sheets in the barrel and 94 in the endcaps. They have a thickness of 20 and 5 mm resp. corresponding to $4.7\,\lambda$ (barrel) and $11\,\lambda$ (endcaps). The interaction length λ is 7.5 cm.

To achieve a good energy resolution the sampling thickness for active and passive absorber layers are kept as close to that required for compensation (equal electromagnetic and hadronic responses). However, in order to achieve the required electromagnetic resolution (see Table 1), compensation could not be realized completely. Software energy-weighting will be applied to regain compensation. The constant term dominates the resolution above 100 GeV. An ambitious goal is to keep it below 1 % and 4 % resp.

To achieve a good energy flow measurement, which is important for jet reconstruction, the calorimeter has a high granularity: $0.9^\circ \times 0.9^\circ$ and $2^\circ \times 2^\circ$ for the electromagnetic and hadronic part resp. The longitudinal segmentation of the towers will be at least three readout cells. The total number of read-out cells sums up to 342,220. For the electromagnetic part, an angular resolution of 0.9 (0.6) mrad is expected at 90° (170°). Hermeticity is required for missing energy measurements, a characteristic signature for supersymmetric particles and neutrinos. The angular range covered is between 4.83° and 175.15°, the instrumented iron goes down to 4°.

As an example for the performance, Fig. 6 shows the energy resolution for single pions and jets from a GEANT simulation of the proposed calorimeter.[5] The resolution obtained matches well the design goals.

5. Detector Performance

The detector performance was tested on a few reference reactions. Among these,

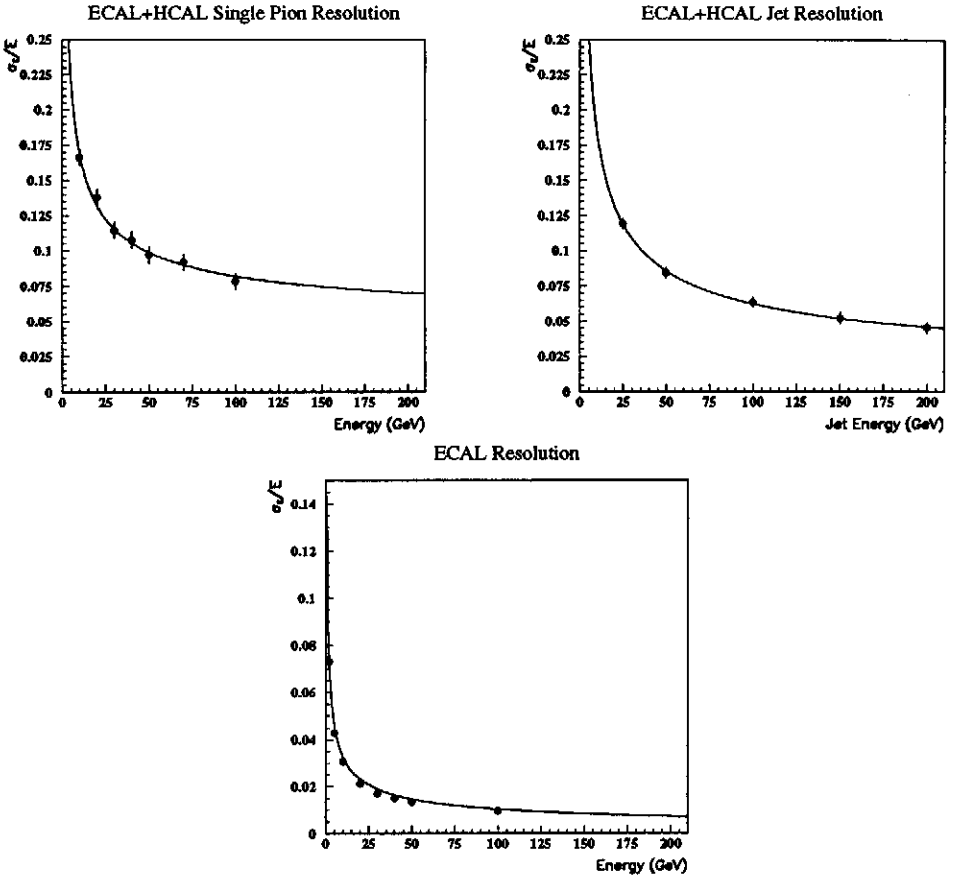

Fig. 6. Single-pion energy resolution (top left), jet energy resolution (top right) and electromagnetic energy resolution (bottom) as a function of particle energy from a GEANT simulation of the calorimeter.

the results of three studies are presented to give an impression of the physics analysis power of the proposed detector: $e^+e^- \to t\bar{t}$ at threshold, $e^+e^- \to HZ$ at $\sqrt{s} = 360\,\mathrm{GeV}$, and $e^+e^- \to \tilde{\chi}_1^+\tilde{\chi}_1^-$ at $\sqrt{s} = 500\,\mathrm{GeV}$. The analysis are described in detail in Ref. 1. It was performed by simulating the processes with reasonable generators,[6] the detector response was simulated using a smearing code.[7] If necessary, a more detailed study of the detector response using GEANT was included.

Top The study of the top at threshold tests the ability of the detector to resolve multijet events and to measure the invariant masses, to identify b-jets, and to cope with the beamstrahlung related background. Due to the high decay rate of the top, toponium states do not form. At threshold, the cross section simply rises from 0.1 to 0.7 pb within about 6 GeV, without a typical resonance behavior. In addition, the shape is distorted by initial state radiation and due to the center-of-mass energy smearing effect of the beamstrahlung. The analysis takes this into

account. An energy scan at threshold ($\sqrt{s} = 350\,\mathrm{GeV}$) with nine points in steps of 1 GeV collecting $5\,\mathrm{fb}^{-1}$ at each point is simulated. The observables are the total production cross section, the momentum distribution, and the forward-backward asymmetry. They are used in a χ^2-fit to determine the top mass together with the strong coupling constant α_S. The analysis assumes a very good measurement of the luminosity spectrum (see also Ref. 2). Figure 7 shows the $1\,\sigma$ contour in the m_t-α_S plane. The overall precision of the top mass and α_S measurements are expected to be $\Delta m_t \leq 110\,\mathrm{MeV}$ and $\Delta\alpha_S \simeq 0.003$ resp. The measurement of the cross section dominates the result, the momentum distribution measurement gives a significant improvement, whereas the asymmetry measurement only contributes to a smaller extent.

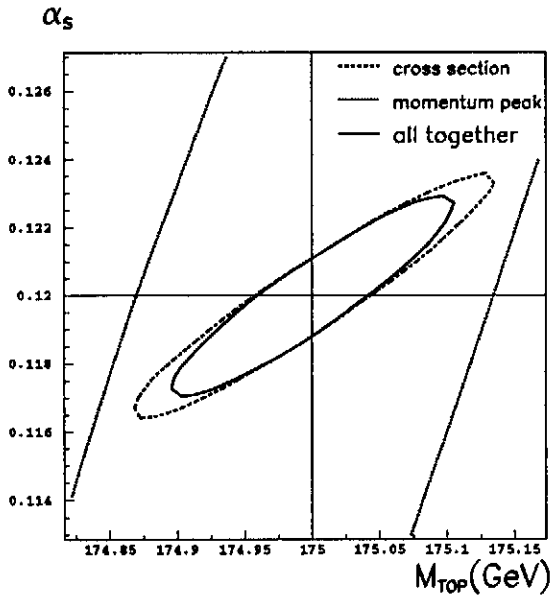

Fig. 7. $1\,\sigma$ contours in the top mass versus α_s plane which is expected to be obtained with the measurement of the cross section and the top momentum distribution in a threshold scan.

Higgs The discovery and study of the Higgs boson is one of the primary motivations for high energy physics projects in the TeV range. At e^+e^- colliders, the main production mechanism for moderate mass Higgs bosons is Higgs-strahlung off the Z boson. The recoiling Z is mono-energetic allowing to reconstruct the Higgs mass from the Z energy. The detection of the Higgs in this channel does not depend on its decay products and thus provides a very powerful searching tool. It also allows study of the Higgs decay mechanism in detail, which is a crucial test of Higgs models.

To test the detector performance, two different Higgs masses, 120 and 140 GeV at two different center-of-mass energies, 360 and 500 GeV were chosen. The analysis requires good jet-jet invariant mass resolution and a precise determination of the

energy and the directions of the hadronic jets; jet flavor tagging is essential. In addition, a very good momentum determination for fast di-leptons from Z decays is required in order to achieve good missing and recoil mass resolution.

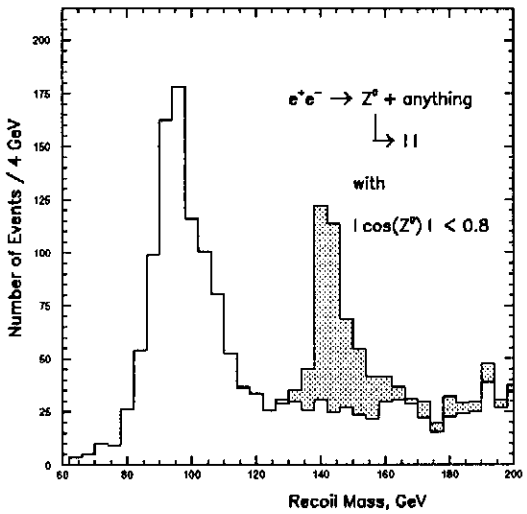

Fig. 8. The dilepton recoil mass distribution showing the signal of a 140 GeV Higgs boson produced together with the Z at $\sqrt{s} = 360\,\text{GeV}$ for an integrated luminosity of $50\,\text{fb}^{-1}$.

As an example, Fig. 8 shows the recoil mass distribution for Higgs-strahlung events, where the Z decays into two charged leptons (for a Higgs mass of 140 GeV, $\sqrt{s} = 360\,\text{GeV}$, and for $50\,\text{fb}^{-1}$). The recoil mass of two isolated fast tracks is calculated. They are checked for consistency with a decay from a Z. With this technique,[8] an integrated luminosity of only $10\,\text{fb}^{-1}$ is required to detect the Higgs boson with a reasonable signal to background ratio. With $50\,\text{fb}^{-1}$ the Higgs production cross-section can be measured with a precision in the order of 5 %. For more details on this analysis see Ref. 1.

Chargino As the last example, the study of chargino pair production to determine the chargino and neutralino masses is discussed. As a reference reaction, the following decay mode is used: $e^+e^- \to \chi_1^+ \chi_1^- \to \chi_1^0 \ell \nu \, \chi_1^0 q\bar{q}'$. The experimental signature is a final state with an isolated lepton and two hadronic jets plus missing energy from the escaped neutralinos. This reaction is therefore an excellent test of the di-jet mass resolution of the detector, its hermeticity for missing energy measurements, and its lepton identification capability. Fig. 9 shows the di-jet energy spectrum obtained for an integrated luminosity of $50\,\text{fb}^{-1}$ at $\sqrt{s} = 500\,\text{GeV}$ ($m_{\chi_1^\pm} = 168.2\,\text{GeV}, m_{\chi_1^0} = 88.1\,\text{GeV}, m_{\tilde{\nu}_e} = 304.0\,\text{GeV}$). The shape is distorted due to the event selection criteria, detector resolution and initial state radiation. Beamstrahlung effects are sizeable and are accounted for. The background from WW-decays is small. A two parameter maximum likelihood fit (also shown in

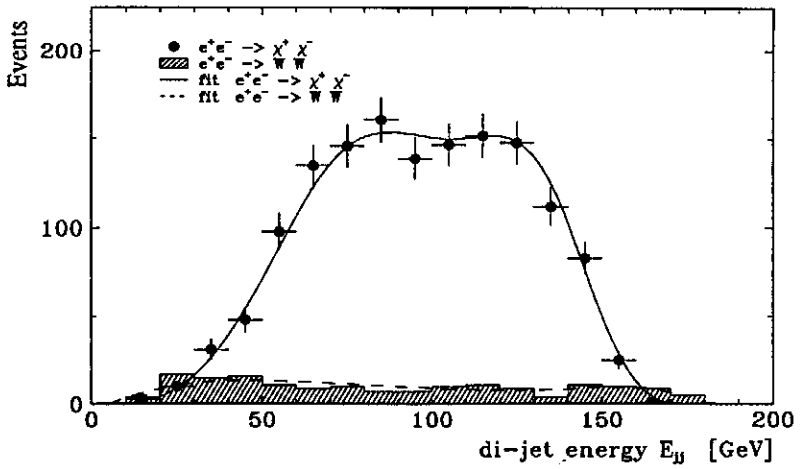

Fig. 9. Di-jet energy spectrum distribution of the chargino pair production $e^+e^- \to \chi_1^+ \chi_1^- \to \chi_1^0 \ell \nu \, \chi_1^0 q\bar{q}'$ (• and —) for an integrated luminosity of $50\,fb^{-1}$. Also shown is the background from $e^+e^- \to W\,W$ events (histogram and – –).

Fig. 9) to the di-jet energy spectrum is used to determine the chargino and neutralino masses.[9] With the present detector, they can be measured to a statistical precision of 0.7 %. With an additional threshold scan, the mass resolution can be improved to the 100 MeV level.

6. Conclusion

The joint ECFA/DESY Study "Physics and Detectors for a Linear Collider" has proposed a detector for a future e^+e^- collider in the TeV range. The detector is designed as a large general purpose detector incorporating the well proven detector concepts of tracking, electromagnetic and hadronic calorimeters, and muon detection. Although, the concept is derived from existing detectors, the performance of all detector components have to be significantly improved compared to e.g. the LEP detectors, namely the tracking performance including the vertex determination, the granularity of all major detector parts, and the performance of the hadronic calorimeter. Due to the expected background from beamstrahlung, a special masking system is introduced in the forward region, which protects the detector from most of the machine induced background. The detector performance was tested with detailed simulations of reference reactions. None of these studies revealed a major limitation, although the masking system unavoidably limits the performance in parts of the forward region. It has been shown, that the detector is adequate to cover the rich physics programme expected. In the future, more detailed studies of the complete detector as a unit and of critical detector parts will be performed to refine the design and to identify regions where further R & D is required.

7. Acknowledgment

I would like to thank U.C. Müller, H.J. Schreiber, D. Schulte, R. Settles, and M. Tonutti for their helpful discussions on various detector components. Furthermore I would like to express my thanks to the organizers of this very interesting workshop in an agreeable atmosphere.

References

1. R. Brinkmann, G. Materlik, J. Rossbach, A. Wagner (ed.), *Conceptual Design of a 500 GeV e^+e^- Linear Collider with Integrated X-ray Laser Facility*, DESY 97-048 and ECFA 97-181, 1997.
2. S. Schreiber, *The TESLA Project*, these proceedings.
3. D. Schulte, *Study of Electromagnetic and Hadronic Background in the Interaction Region of the TESLA Collider*, TESLA Report 97-08, DESY 1997.
4. ALEPH Collab., D. Buskulic et al., *Performance of the ALEPH Detector at LEP*, Nucl. Instrum. and Methods A360 (1995) 481.
5. See also "ECFA/DESY Study of Physics and Detector for a Linear Collider", http://www.desy.de/conferences/ecfa-desy-lc96.html, proceedings to be published as DESY 97-123E.
6. See http://www.thep.lu.se/tf2/staff/torbjorn/LCphysgen.html
7. H.J. Schreiber, SIMDET, available upon request from schreibe@ifh.de
8. P. Grosse-Wiesmann, D. Haidt and H.J. Schreiber, DESY 92-123A;
   P. Janot, LAL 93-38;
   H.D. Hildreth, T.L. Barklow and D.L. Burke, Phys. Rev. D49 (1994), 3441.
9. T. Tsukamoto et al., Phys. Rev. D 51 (1995) 3153.